Available online at www.sciencedirect.com
ScienceDirect
International Journal of Mass Spectrometry 265 (2007) 176–181
International Journal of Mass Spectrometry
www.elsevier.com/locate/ijms

Collisional cooling in a quadrupole ion trap at sub-ambient temperatures

Philip M. Remes, Gary L. Glish *

Department of Chemistry, University of North Carolina at Chapel Hill, Chapel Hill, NC 27599-3290, USA

Received 1 November 2006; received in revised form 7 February 2007; accepted 7 February 2007
Available online 11 February 2007

Abstract

Quadrupole ion traps have been used successfully as ion storage devices for infrared multiphoton dissociation (IRMPD) experiments. Recently there has been interest in doing low temperature action spectroscopy experiments using ion traps as detectors for IRMPD spectroscopy. Cooling the trapping electrodes has the effect of cooling the trapped ions to the same internal temperature, because quadrupole ion traps operate at He bath gas pressures high enough to produce equilibrium ion internal energy distributions. It has previously been shown that collisions of the ions with the bath gas cool the ions' internal vibrational modes at a rate that competes with IRMPD excitation at ambient temperatures. To investigate the implications of doing IRMPD in a quadrupole ion trap at lower trapping temperatures, the present study measures the collisional cooling rate constants at sub-ambient temperatures down to 25 K. The change in collisional cooling rate constant with trap temperature is correlated to the increased energy needed to dissociate the ions at these lower trap temperatures. It is found that both the energy needed to effect dissociation and the collisional cooling rate increase exponentially as trap temperature drops.

Keywords: IRMPD; Collisional cooling; Quadrupole ion trap; Low temperature

1. Introduction

Since the development of the quadrupole ion trap as a commercial instrument, helium gas (He) has been introduced into the trapping volume at a relatively high pressure (∼1 mTorr) to damp the ions' kinetic energy [1]. The high pressure of neutral gas in a quadrupole ion trap makes it unique among mass analyzers in that the ion/neutral collision frequency is quite high; it has been estimated at 20 collisions per millisecond during normal storage conditions [2]. The initial goals of kinetic energy damping on ion trap performance were increased mass resolving power and increased sensitivity. The addition of external ion sources to ion traps allowed for the analysis of high molecular weight ions produced by electrospray ionization (ESI) [3] and matrix assisted laser induced desorption ionization (MALDI) [4–6]. However, to trap the injected ions, collisional damping, and thus the helium bath gas, is necessary.

While the objective of adding the bath gas is to reduce the kinetic energy of an ion, the internal energy of the ion is also affected such that during normal storage periods it may be described by a Boltzmann distribution at the temperature of the bath gas [7–11]. Whenever an ion is activated, such as during collision induced dissociation (CID) [12–14] or infrared multiphoton dissociation (IRMPD) [15–18], the collisions with the bath gas act to cool the ion back down to thermal internal energy. It has been proposed that the average internal temperature decrease per collision increases as the ion is activated above the temperature of the bath gas [19]. The collisional cooling rate constant has been measured previously for the peptide leucine enkephalin at a series of trapping pressures and temperatures, at or above ambient temperature [20]. The pseudo first-order rate constant for ambient temperature and 1 mTorr He was 400 s^{-1}. This cooling process has been shown to effectively compete with activation by IRMPD; thus, many larger ions such as peptides are difficult to dissociate under normal operating conditions [15].

Recently there has been increased interest in infrared (IR) action spectroscopy techniques, such as IRMPD spectroscopy, that couple tunable lasers with mass spectrometers [21–31]. Instead of trying to make a direct absorbance measurement, these experiments monitor a chemical process dependent on the absorbance cross section at a particular wavelength, typically photodissociation of the ion. The fragment ion abundance is plotted versus laser wavelength to give an IR spectrum. Several of these studies have employed electrodynamic trapping devices

* Corresponding author. Tel.: +1 919 962 2303
E-mail address: glish@unc.edu (G.L. Glish).

1387-3806/$ – see front matter © 2007 Elsevier B.V. All rights reserved.
doi:10.1016/j.ijms.2007.02.004

with cooled electrodes [32–34]. Doing spectroscopy on ions at low temperatures simplifies spectra by reducing the number of hot vibrational bands. Sensitivity at a particular laser wavelength is also increased because the ions are concentrated into a smaller number of energy states.

A quadrupole ion trap instrument was recently built in our lab for the purpose of doing IRMPD spectroscopy experiments at low (<100 K) temperatures. One of the important questions in the design of this instrument was to what extent collisional cooling would limit the ability to perform experiments at these low temperatures. The fact that trapped ions equilibrate with the He bath gas is simultaneously an advantage and a disadvantage: low ion internal temperatures can be reached, which is favorable for spectroscopy, at the price of higher collisional cooling rates and thus a need for greater laser powers to effect dissociation. The purpose of this work is to quantify the effect of collisional cooling at sub-ambient temperatures. To this end, two experiments were performed. The first experiment demonstrates the relationship between the energy required for dissociation and ion temperature. Naturally, as the temperature of the ion decreases, the amount of input energy required to reach a given internal energy will increase. It is not immediately obvious, however, if the input energy to temperature relationship should be linear, or follow some other dependence. Therefore, fragmentation efficiency curves showing the extent of dissociation versus CID voltage were obtained for various peptide ions at a series of low trap temperatures. The second experiment quantifies the collisional cooling rate constant for the ion *n*-butylbenzene at a series of low trap temperatures. The two experiments are then compared and the input energy required to reach a certain internal energy can be correlated with a collisional cooling rate constant.

2. Methods

2.1. Instrumentation

Experiments were performed on a home-built quadrupole ion trap mass spectrometer (QITMS) designed for laser spectroscopy applications. The details of this instrument will be discussed in a later publication. Briefly, this QITMS uses a Finnigan ITD set of electrodes mounted on a Sumitomo RDK-408S 10 K closed cycle helium refrigerator with the specific goal of cooling down the electrodes to low temperatures for IR spectroscopy experiments.

When the instrument is configured for nano-ESI, sample solutions are introduced into a pulled glass capillary which contains a grounded wire. An ESI voltage of −1100 V is applied to a metal cap on a 20.32 cm long, 0.60 cm diameter glass transfer capillary with a ∼400 μm diameter hole through the center and the atmospheric end flared inwards for ease of needle alignment [35]. The ions are transferred from the capillary to the ion trap via an octapole ion guide. When analysis of ions produced by electron ionization (EI) is desired, the nano-ESI source and transfer optics are replaced with a TSQ 70 EI source. Base pressure in the source region is 8×10^{-8} Torr. Electron energy is set to 70 eV, and the EI source is floated at 20 V. Sample vapors are leaked into the source at $\sim 2 \times 10^{-6}$ Torr through a sidearm fitted with a metering valve.

2.2. Samples

The protonated molecules of the peptides GHK, YGGFL and FLLVPLG were produced by nano-ESI. The molecular ion of *n*-butylbenzene was produced by EI. The nano-ESI samples' concentrations were 100–200 μM in 75/20/5 methanol/water/acetic acid. YGGFL, GHK, and *n*-butylbenzene were purchased from Sigma–Aldrich (St. Louis) and FLLVPLG was custom synthesized by Bayer Corp. All samples were used without any purification.

2.3. CO_2 laser

The CO_2 laser used for IRMPD is a 10.6 μm, continuous output, 0–100 W, Synrad Firestar f100. The laser is triggered by a TTL signal from the instrument software at the appropriate time in the experiment. The laser beam is delivered with 3 silicon mirrors and focused to the center of the ITMS with a 38.1 cm focal length ZeSe lens. Laser power is set by a manufacturer supplied digital controller. Power was generally set at ∼10–30 W, depending on pressure and temperature.

2.4. Mass spectrometry

Ions were gated into the ion trap with a high voltage switching circuit for ∼10–50 ms for nano-ESI, and 1–5 ms for EI. The gating circuit has no provision for automatic gain control [36], so the gate time was chosen to give a moderately high ion signal, but not so high that any space charge effects, indicated by mass shifts, were apparent. To isolate the ions of interest, lower mass ions were ejected from the trap by raising the rf level to the appropriate value, and any higher mass ions (mostly $[M+Na]^+$) were ejected by applying a supplementary ac voltage to the end-cap electrodes at the appropriate frequency and ramping down the rf level. The isolated ions were then allowed to cool for 30 ms at a q_z value of 0.30 to ensure equilibrium kinetic and internal energy levels. This q_z value was used for all IRMPD and CID experiments. Although a q_z value of 0.30 is higher than is customarily used in many IRMPD experiments, we have observed that improved IRMPD efficiencies can be realized at higher q_z values, a phenomenon which will be discussed in a future publication. A q_z of 0.30 also optimized the efficiencies obtained for CID.

Collisional cooling rates were measured for *n*-butylbenzene by the two-pulse method described by Asamoto and Dunbar [37]. After equilibrating with the He bath gas, the ions are irradiated by two 3 ms pulses from the CO_2 laser, separated by a variable delay time. The delay time between laser pulses was increased sequentially from 0 ms to a time great enough for the ions to finish cooling, generally a time between 4 and 50 ms, depending on He pressure. The cooling time was varied automatically from spectrum to spectrum under computer control. The experimental timing diagram is shown in Fig. 1a. A mass

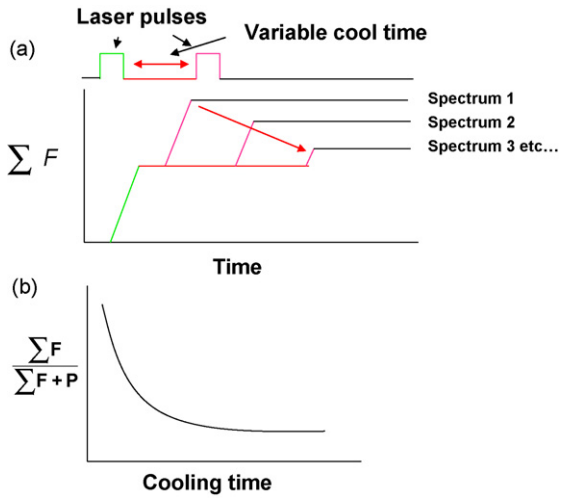

Fig. 1. (a) Experimental timing diagram for determination of collisional cooling rate constant; (b) theoretical cooling curve showing fragmentation efficiency decreasing as cooling time is increased.

spectrum is obtained at each of a series of cooling times, and fragmentation efficiency is plotted as a function of cooling time as in Fig. 1b. Fragmentation efficiency is defined in equation (1), where $\sum F$ is the sum of the fragment ion intensities and P is the parent ion intensity from the MS/MS spectrum.

$$\mathrm{FE} = \frac{\sum F}{\sum F + P} \tag{1}$$

The collisional cooling rate can be found by fitting the fragmentation efficiency plot to an exponential decay, which will be discussed in more depth in the following theoretical Section 3. The laser power is set such that when the variable cool time is 0, fragmentation efficiency is ~50%. Setting a constant initial fragmentation efficiency ensures that ions are relaxing from a constant maximum internal energy level. Each recorded spectra was the average of 25 scans. Each curve in the data reported here is the average of 15 separate experiments, and error bars are calculated as 95% confidence intervals.

CID is performed by applying a supplementary ac excitation voltage to the QITMS endcap electrodes at the same frequency as the secular frequency of oscillation of the parent ion to be dissociated. The parent ion gains kinetic energy through application of the excitation voltage, such that collisions with the He bath gas are able to dissociate the ion. Plots of fragmentation efficiency versus excitation voltage were obtained at various trap temperatures, at an estimated He pressure of 3 mTorr. Because the trapping volume is enclosed in a conductance limiting copper box, the He pressure in the trapping volume is higher than what is measured by the pressure gauge. A relation between the trapping volume pressure and main chamber pressure was established by comparing collisional cooling rates at two experimental conditions: the rates when the electrodes were enclosed were compared to those rates measured with the electrodes not enclosed (tops of boxes removed). The correction factor is approximately 14 times the pressure read on the pressure gauge. The excitation voltage applied to the endcap electrodes was varied under computer control such that spectra were recorded with fragmentation efficiencies from 0 to 100%. Each recorded spectrum was the average of 40 scans, and 6 separate experiments were averaged to produce each fragmentation efficiency curve.

3. Theory

The possible mechanisms of energy transfer in the IR activation experiment have been described before [19,20] and are outlined in the following equations, where M^+ is the singly charged parent ion, M^{+*} is the activated parent ion, and He is helium bath gas.

$$M^+ + He \xrightarrow{k_{CA}} M^{+*} + He \tag{2}$$

$$M^+ + h\upsilon \xrightarrow{k_{IR}} M^{+*} \tag{3}$$

$$M^{+*} + He \xrightarrow{k_{ccool}} M^+ + He \tag{4}$$

$$M^{+*} \xrightarrow{k_{radiative}} M^+ + h\upsilon \tag{5}$$

$$M^{+*} \xrightarrow{k_{dissociation}} \text{products} \tag{6}$$

The total rate of change of M^{+*} is the summation

$$\frac{d[M^{+*}]}{dt} = k_{CA}[M^+][He] + k_{IR}[M^+][h\upsilon] - k_{ccool}[M^{+*}][He] - k_{radiative}[M^{+*}] - k_{dissociation}[M^{+*}] \tag{7}$$

where the rate constants, k_{CA}, k_{IR}, k_{ccool}, $k_{radiative}$, and $k_{dissociation}$, respectively, refer to the rates of collisional activation, infrared activation, collisional cooling, radiative emission, and unimolecular dissociation. Two energy transfer processes may be disregarded for the present experiments; the rate of collisional activation and the rate of radiative emission. The collisional activation rate is zero because no resonance excitation is used and the ions are allowed to reach equilibrium kinetic/internal energy levels before being photoexcited. The radiative emission rate constant for *n*-butylbenzene has been measured previously as being 0.97 s^{-1} [38]. This rate constant is 2–4 orders of magnitude smaller than the collisional cooling rate constants obtained in the present study, and can thus be ignored. During the two laser excitation pulses, the change in $[M^{+*}]$ is then given in Eq. (8)

$$\frac{d[M^{+*}]}{dt} = k_{IR}[M^+][h\upsilon] - k_{ccool}[M^{+*}][He] - k_{dissociation}[M^{+*}] \tag{8}$$

The two-pulse method uses the second laser pulse to gauge the rate of cooling occurring between the laser pulses, where collisional cooling is the only significant energy transfer process taking place. With no cooling time between the two pulses, the ion will reach a certain maximum internal energy and a corresponding maximum level of dissociation. As the two pulses are separated more in time, the M^{+*} population is depleted through collisional cooling, and the number of fragments formed decreases. Monitoring fragmentation efficiency is therefore a way of following the evolution in $[M^{+*}]$. The collisional cooling rate is subsequently given by Eq. (9), and the pseudo first-order

rate constant is given by Eq. (10).

$$\frac{d[M^{+*}]}{dt} = -k_{ccool}[M^{+*}][He] \quad (9)$$

$$k'_{ccool} = k_{ccool}[He] \quad (10)$$

Eq. (9) describes an exponential decay process of the form of Eq. (11).

$$\frac{[M^{+*}]}{[M_0^{+*}]} = e^{-k_{ccool}[He]t} \quad (11)$$

$[M_0^{+*}]$ is the initial population of activated ions and t is cooling time. Fragmentation efficiency is being taken as a measure of $[M^{+*}]$, therefore plots of FE/FE_0 were fit to an exponential decay equation and the rate constant was obtained from the curve of best fit. FE_0 is fragmentation efficiency at zero cooling time.

4. Results and discussion

Plots of fragmentation efficiency versus CID excitation voltage for protonated leucine enkephalin are shown in Fig. 2a. When the CID voltage required to reach 50% fragmentation efficiency (a constant internal energy) is plotted versus ion trap temperature, the exponential shaped curves shown in Fig. 2b are obtained for the three peptides studied. The exponential decay fitting parameters for the data in Fig. 2b are given in Table 1. These curves follow a trend according to the size of the peptide investigated; the smallest peptide, GHK, requires the least voltage to dissociate at all temperatures, and has the smallest slope, while the biggest peptide, FLLVPLG, requires the most voltage to dissociate, and has the largest slope. This trend makes sense in the RRKM statistical dissociation model, where a larger ion will have more modes to distribute internal energy into, and thus require more energy input to dissociate. When these curves were normalized for degrees of freedom (data not shown), the curves for the smaller peptides overlap quite closely, while the curve for FLLVPLG is slightly lower than the other two. Naturally it is expected that as ion temperature is decreased the energy required for dissociation increases. However, the fact that the curves in Fig. 2b are exponential at very low temperatures is not expected. Previous studies have shown a relatively linear relationship of CID voltage to internal energy gain [39].

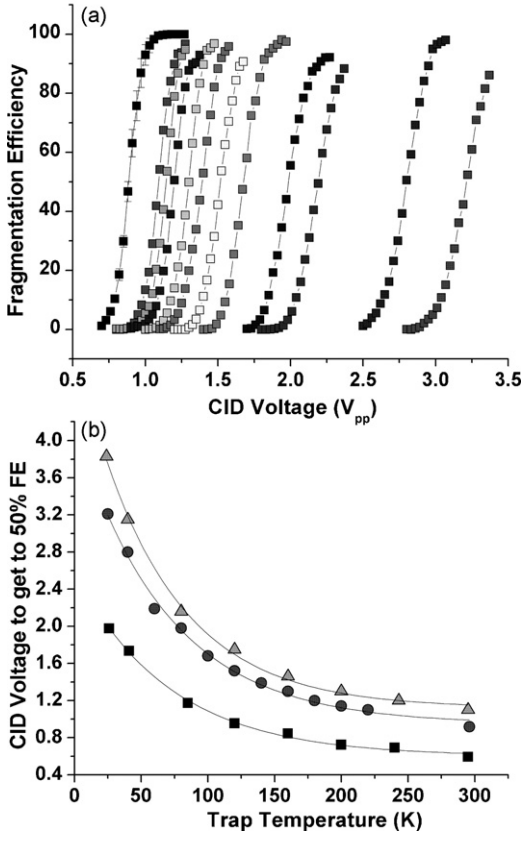

Fig. 2. (a) Fragmentation efficiency curves for $[YGGFL + H]^+$ at various trap temperatures from 295 K (left side) to 25 K (right side). Error bars are included in only the 295 K data to show typical reproducibility. (b) CID voltage required to reach a constant fragmentation efficiency (a constant internal energy) at various trap temperatures. Squares are for $[GHK + H]^+$, circles for $[YGGFL+]^+$, and triangles for $[FLLVPLG + H]^+$, and the black line is an exponential decay fit to the data.

Table 1
Parameters for exponential fit to $y = y_0 + A\,e^{-Temp/C}$

Species	y_0	A	C	R^2
GHK	0.60	1.99	71.2	0.998
YGGFL	0.95	3.2	68.8	0.996
FLLVPLG	1.12	3.92	62.6	0.998

Internal energy considerations actually suggest that the slope of the curves in Fig. 2b should get less steep at very low temperatures. The latter point is demonstrated in Fig. 3, where the average internal energy for *n*-butylbenzene molecular ion is plotted in squares as a function of ion internal temperature using equation (12) for temperatures from 10 to 900 K.

$$\langle E \rangle = \frac{1}{Q}\int_0^\infty \rho(E) E\, e^{-E/kT}\, dE \quad (12)$$

where Q is the vibrational partition coefficient, $\rho(E)$ the density of states at internal energy E, k Boltzmann's constant, and T is the internal temperature of the ion. Density of states were calculated by the established procedure [40] using vibrational frequencies

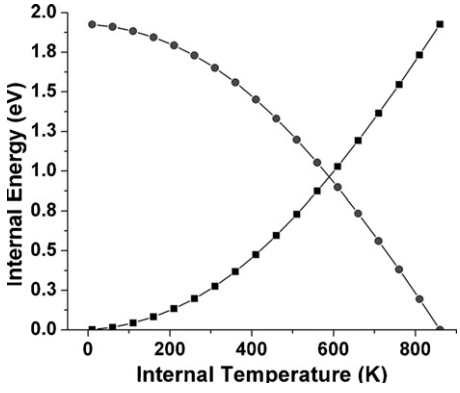

Fig. 3. Relationship between internal energy and internal temperature for *n*-butylbenzene molecular ion (squares). The circles are the energy needed to raise the ion's temperature to 860 K.

calculated at the B3YLP/6-31G(d) level in Gaussian 03 [41]. At lower internal temperatures, a small input of energy results in a larger increase in internal temperature. This is because at lower internal temperatures there are fewer states throughout which to distribute energy, and so the effective temperature of the ion changes faster. Density of states increases very quickly with ion internal temperature, so that at higher internal temperatures there are more ways to distribute energy throughout the ion. The result is a slower increase in effective temperature with energy input. The curve with circles in Fig. 3 shows the shape that might be expected for CID voltage versus ion trap temperature, based on the above argument. The circles assume 860 K as the critical dissociation *temperature* (the onset of parent ion fragmentation) and denote the internal energy that needs to be added to the ion to reach the critical dissociation *energy* of 1.9 eV.

The fact that the relationship between CID voltage and internal temperature in Fig. 2b is exponential suggests that another process must be involved, and collisional cooling is an obvious candidate. Fig. 4a shows an experimental cooling curve for *n*-butylbenzene, fit to an exponential decay equation. Fig. 4b is a composite graph of pseudo first-order rate constants determined at a range of He pressures and trap temperatures. A linear relationship between the collisional cooling rate constant and pressure has been demonstrated before in an ion cyclotron resonance mass spectrometer; however, these data were obtained at much lower pressures [42]. The curves in Fig. 4b appear to increase exponentially with pressure, especially at lower trap temperatures. The same exponential increase with pressure was observed in a previous study in a QITMS [20]. At the very lowest pressures, a steady-state ion internal energy was reached within 50 ms. This time to reach equilibrium decreases rapidly with increasing pressures, and at most normal operating pressures, equilibrium is reached in less than 10 ms.

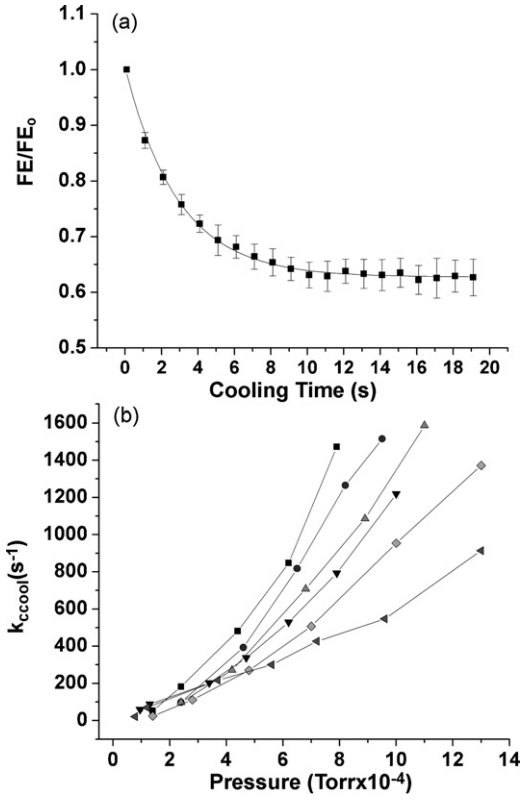

Fig. 4. (a) Experimental cooling curve for *n*-butylbenzene at 5.8×10^{-4} Torr He, 295 K. The pseudo first-order rate constant was 334 s^{-1} for this curve. Squares are experimental points with 95% confidence bands. The solid curve is an exponential decay fit with $R^2 = 0.996$. (b) Pseudo first-order collisional cooling rate constants vs. pressure at 36 K (squares), 70 K (circles), 100 K (up triangle), 150 K (down triangle), 200 K (diamond), and 296 K (45° triangle).

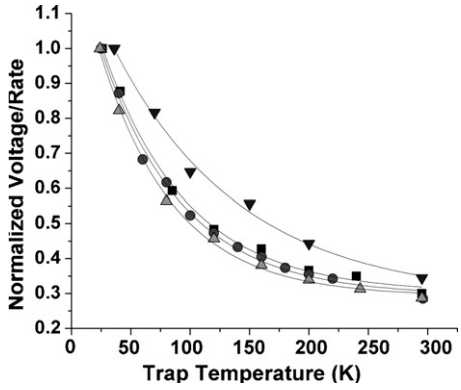

Fig. 5. Comparison of collisional cooling rate constants vs. trap temperature and CID voltage required to reach a constant internal energy vs. trap temperature. The CID data are normalized to the highest voltage, and the cooling rate data is normalized separately to the highest rate constant. Squares are for $[GHK + H]^+$, circles for $[YGGFL+]^+$, up-triangles for $[FLLVPLG + H]^+$, down-triangles for collisional cooling rate constants of *n*-butylbenzene, and the black curves are an exponential decay fit to the data.

In Fig. 5, the pseudo first-order rate constants for collisional cooling from Fig. 4b at a constant pressure of 7×10^{-4} Torr are normalized and plotted on the same trap temperature axis as the normalized CID data from Fig. 2b.

It is apparent in Fig. 5 that the voltage curves start to increase rapidly below ~100 K, the same trap temperature where the collisional cooling rate constant increases most rapidly. It is natural to conclude based on these data that the collisional cooling process is responsible for the exponentially increasing energy requirement for dissociation at low trapping temperatures. A possible interpretation of the results comes from the same density of states argument discussed in relation to Fig. 3. If it is assumed that each collision with a He atom takes away a given amount of energy, then at lower ion temperatures that same collision will decrease the ion's internal temperature more than at higher ion temperatures. Again, this would be because at lower ion temperatures there are fewer available energy states, so that a given input/output of energy increases/decreases the ions internal temperature to a greater extent.

5. Conclusions

The CID voltage required to reach a constant internal energy has been determined for a series of protonated peptides at internal temperatures from 25 to 295 K in a QITMS. A greater than linear increase in voltage is needed, especially at trapping temperatures lower than 100 K. Collisional cooling rate constants have also been determined for a combination of pressures and

trap temperatures for the molecular ion of *n*-butylbenzene. Collisional cooling rate constants increase exponentially as trap temperature decreases, which correlates well with the increased voltage needed for CID. Collisional cooling is an important energy transfer process in ion traps, especially at high He bath gas pressures and low trap temperatures. In low temperature IRMPD studies, such as action spectroscopy experiments where an ion must be dissociated in the presence of thermalizing bath gas pressures, it is important to have enough laser power to overcome the collisional cooling effect. We have observed in other experiments, comparing IRMPD efficiencies at different trap temperatures, that the increased laser power needed to dissociate an ion at ambient versus low trapping temperature can be 3 fold or greater. As interest shifts towards studying the structures of larger biomolecules in the gas phase, laser power could be a limiting factor, since generally speaking, larger ions have higher activation energies due to the increased number of degrees of freedom.

Acknowledgements

This work was supported by NSF grant #CHE-0431825. We would like to thank John Peterson and Collin McKinney of the UNC chemistry electronics facility and Freddy Pinero and James Perotti of the UNC chemistry instrument shop for helpful discussions and work done on the low temperature ion trap.

References

[1] G.C.J. Stafford, P.E. Kelley, J.E.P. Syka, W.E. Reynolds, J.F.J. Todd, Int. J. Mass Spectrom. Ion Process. 60 (1984) 85.
[2] R.E. March, Quadrupole ion trap mass spectrometry, in: R.A. Meyers (Ed.), Encyclopedia of Analytical Chemistry, John Wiley & Sons Ltd., Chichester, 2000, p. 11848.
[3] G.J. VanBerkel, G.L. Glish, S.A. McLuckey, Anal. Chem. 62 (1990) 1284.
[4] D.M. Chambers, D.E. Goeringer, S.A. McLuckey, G.L. Glish, Anal. Chem. 65 (1993) 14.
[5] J.D.I. Lennon, G.L. Glish, Anal. Chem. 69 (1997) 2525.
[6] J. Qin, R.J.J.M. Steenvoorden, B.T. Chait, Anal. Chem. 68 (1996) 1784.
[7] D.E. Goeringer, K.G. Asano, S.A. McLuckey, Int. J. Mass Spectrom. 182/183 (1999) 275.
[8] D.J. Butcher, K.G. Asano, D.E. Goeringer, S.A. McLuckey, J. Phys. Chem. A 103 (1999) 8664.
[9] K.G. Asano, D.J. Butcher, D.E. Goeringer, S.A. McLuckey, J. Mass Spectrom. 34 (1999) 691.
[10] W.R. Plass, R.G. Cooks, J. Am. Soc. Mass. Spectrom. 14 (2003) 1348.
[11] P.M. Remes, G.L. Glish, J. Am. Soc. Mass Spectrom., submitted for publication.
[12] S.A. McLuckey, J. Am. Soc. Mass. Spectrom. 3 (1992) 599.
[13] J.N. Louris, R.G. Cooks, J.E.P. Syka, P.E. Kelley, G.C. Stafford, J.F.J. Todd, Anal. Chem. 59 (1987) 1677.
[14] D.J. Douglas, J. Phys. Chem. 86 (1982) 185.
[15] A.H. Payne, G.L. Glish, Anal. Chem. 73 (2001) 3542L 3548.
[16] W. Gabryelski, L. Li, Rapid Commun. Mass Spectrom. 16 (2002) 1805.
[17] B.J. Goolsby, J.S. Brodbelt, Anal. Chem. 73 (2001) 1270.
[18] D.P. Little, J.P. Speir, M.W. Senko, P.B. Oconnor, F.W. McLafferty, Anal. Chem. 66 (1994) 2809.
[19] D.E. Goeringer, S.A. McLuckey, Int. J. Mass Spectrom. 177 (1998) 163.
[20] D.M. Black, A.H. Payne, G.L. Glish, J. Am. Soc. Mass Spectrom. 17 (2006) 932.
[21] L. Mac Aleese, A. Simon, T.B. McMahon, J.-M. Ortega, D. Scuderi, J. Lemaire, P. Maitre, Int. J. Mass Spectrom. 249/250 (2006) 14.
[22] K. Fukui, Y. Takada, T. Sumiyoshi, T. Imai, K. Takahashi, J. Phys. Chem. B 110 (2003) 16111.
[23] B. Chiavarino, M.E. Crestoni, S. Fornarini, O. Dopfer, J. Lemaire, P. Maitre, J. Phys. Chem. A 110 (2006) 9352.
[24] N.C. Polfer, J. Oomens, R.C. Dunbar, Phys. Chem. Chem. Phys. 8 (2006) 2744.
[25] M. Putter, G. von Helden, G. Meijer, Chem. Phys. Lett. 258 (1996) 118.
[26] G. von Helden, I. Holleman, M. Putter, G. Meijer, Nucl. Instrum. Methods Phys. Res. Sect. B Beam Interact. Mater. Atoms 144 (1998) 211.
[27] J. Oomens, G. Meijer, G.v. Helden, J. Phys. Chem. A 105 (2001) 8302.
[28] J. Oomens, A.J.A.v. Roij, G. Meijer, G.v. Helden, Astrophys. J. 542 (2000) 404.
[29] C.D. Thompson, C. Emmeluth, B.L.J. Poad, G.H. Weddle, E.J. Bieske, J. Chem. Phys. 125 (2006) 044310/1.
[30] Z.M. Loh, R.L. Wilson, D.A. Wild, E.J. Bieske, M.S. Gordon, J. Phys. Chem. A 109 (2005) 8481.
[31] R.L. Wilson, Z.M. Loh, D.A. Wild, C.D. Thompson, M.D. Schuder, J.M. Lisy, E.J. Bieske, Phys. Chem. Chem. Phys. 7 (2005) 3419.
[32] K.R. Asmis, G. Meijer, M. Brummer, C. Kaposta, G. Santambrogio, L. Woste, J. Sauer, J. Chem. Phys. 120 (14) (2004) 6461.
[33] M. Brummer, C. Kaposta, G. Santambrogio, K.R. Asmis, J. Chem. Phys. 119 (2003) 12700.
[34] K.R. Asmis, N.L. Pivonka, G. Santambrogio, M. Bruemmer, C. Kaposta, D.M. Neumark, L. Woeste, Science 299 (2003) 1375.
[35] G.L. Glish, R.M. Danell, Electrospray Ionization Device, U.S. Patent No. 6,703,611 (2004).
[36] R.E. March, J.F.J. Todd (Eds.), Quadrupole Ion Trap Mass Spectrometry, second ed., in: J.D. Winefordner (Ed.) Chemical Analysis, vol. 165, John Wiley & Sons, Inc., Hoboken, NJ, 2005, p. 346.
[37] B. Asamoto, R.C. Dunbar, J. Phys. Chem. 91 (1987) 2804.
[38] G.T. Uechi, R.C. Dunbar, J. Chem. Phys. 98 (1993) 7888.
[39] D.E. Goeringer, S.A. McLuckey, J. Chem. Phys. 104 (1996) 2214.
[40] S.E. Stein, B.S. Rabinovitch, J. Chem. Phys. 58 (1973) 2438.
[41] M.J. Frisch, Gaussian 03, Revision C.02, Gaussian, Inc., Wallingford, CT, 2004.
[42] R.C. Dunbar, J. Chem. Phys. 91 (1989) 6080.